2. METHODOLOGY

2.1. Characterisation of plastic materials

2.1.1. Plastic samples

Preliminary selection of materials

The selection of suitable plastics for the manufacturing of SODIS devices was carried out considering mechanical and optical properties as well as production costs. Mechanical properties and production costs were investigated through an exhaustive review of the literature, whereas the optical properties were experimentally measured. The following transparent plastic materials were considered: PS, PVC, PP, PE, PET, PC, and PMMA. Their mechanical resistance, photostability, durability, and production cost were studied.

Impact of weathering on materials properties and SODIS efficacy A deeper study of the weathering of plastic SODIS containers and their impact on their lifetime and the disinfection efficacy was carried out through the accelerated ageing of plastics selected as suitable candidate materials and used in current SODIS processes:

- PMMA: obtained from static solar reactors used to treat rainwater in South Africa and Uganda (Martínez-García ***et al.,*** 2021; Reyneke ***et al.,*** 2020). This system consisted of a 20 L tubular reactor made with UV-transparent PMMA coupled to an aluminium compound parabolic collector.

- PET: extracted from transparent 25 L jerrycans used for the solar disinfection of drinking water in rural villages in Mekelle, in Northern Ethiopia ("WaterSPOUTT project," 2022).

- PP1: extracted from transparent buckets used in rural villages of Southern Malawi (Morse ***et al.,*** 2020; Polo-López ***et al.,*** 2019). A peculiarity of this PPI is that it contains 1% by weight of UV-stabiliser.

- PP2: this plastic is classified as poorly photostable and was extracted from transparent 10 L jerrycans manufactured in the UK and planned to be deployed for solar disinfection of water in rural India (TotalEnergies, 2022).

Table 2.1 summarises the techniques used to analyse the mechanical, physicochemical, and optical properties of the aged materials. These techniques are explained hereafter.

Table 2.1: Summary of the techniques used to analyse the mechanical (MP), physicochemical (PCP), and optical properties (OP) of the aged materials.

	PMMA	PET	PP1	PP2
MP	Flexural test	Tensile test	Tensile test	Tensile test
PCP	FTIR	FTIR	FTIR	FTIR
			DSC	DSC
			GPC	GPC
OP	UV-Vis spectrophot.	UV-Vis spectrophot.	UV-Vis spectrophot.	UV-Vis spectrophot.

2.1.2. Measurement techniques

Ageing test

Plastic samples selected for the second study were aged according to the standard ISO 4892-2 procedure using the Atlas Weather-Ometer Ci4000. The system was equipped with a xenon lamp light and type S borosilicate glass inner and outer filters that simulates the ultraviolet and visible sunlight region. The samples were exposed to weathering cycles under continuous irradiation with an intensity of 0.75 W • m^{-2} at 340 nm for 8 weeks (3.6 MJ • m^{-2} • nm^{-1}). This radiation dose matches with the annual dose received in Mekelle (4.0 MJ • m^{-2} • nm^{-1} (Moreno-SanSegundo ***et al.,*** 2021) or in Miami, USA (3.0-4.0 MJ • m^{-2} • nm^{-1} (Kuvshinnikova ***et al.,*** 2019)). Thus, each week of accelerated ageing corresponds to one month and a half of solar exposure in natural conditions.

Tensile test

Tensile properties for PP1, PP2, and PET were measured according to a modified ISO527 method. The tensile bars used were type 5A. Before testing, the samples were acclimatised at 23°C/50% RH for at least 48 h. The samples were tested on an MTS Alliance RT/5 tensile tester. The clamp length was 50 mm, and the test speed 20 mm/min. The percentage elongation and nominal strain at break were also measured, and yield properties were used to estimate Young's modulus with the extensometer. Each sample was tested in triplicate and the values were averaged.

Flexural test

Flexural properties for PMMA were tested on an MTS Insight machine with a 30 kN load capacity. Flexural tests (under three-point bending configuration) were carried out according to a modified ISO178. The radius of the two supports and central loading edge was 5.0 mm, and the test speed was 2 mm/min. The difference with the original ISO standard was the dimensions of the used bars, which had a rectangular shape of 10×30 mm, and 3 mm of thickness. The PMMA supplier delivered the samples already cut in this way, which is why the mechanical properties of PMMA were measured by flexural tests rather than tensile tests. Before testing, the samples were acclimatised at 23°C/50% RH for at least 48 h. Each sample was tested in triplicate and the values were averaged.

Fourier transform infrared spectroscopy (FTIR)

FTIR on all the plastics was performed using an FTIR Varian Excalibur Series 3100 spectrometer in attenuated total reflection (ATR) mode for 32 scans. The spectra were collected in the 600-4000 cm^{-1} range with a resolution of 2 cm^{-1}. The carbonyl index was calculated from the ratio between the absorbance at 1715 cm^{-1} (maximum point for the carbonyl group) and the absorbance at 974 cm^{-1} for the PMMA and the PPs and 725 cm^{-1} for the PET (the absorbance stayed constant at these wavelengths with the weathering). The crystallinity index was calculated for the PPs by the ratio between the absorbance at 998 cm^{-1} (isotactic polypropylene band (Prabowo ***et al.,*** 2017)) and the absorbance at 974 cm^{-1}.

Differential scanning calorimetry (DSC)

DSC was used to evaluate the thermal properties of the PPs samples of weeks 0, 2, 4, and 8 of ageing using a DSC Mettler-822e. Each sample (8-9 mg) underwent three successive cycles (heating-cooling-heating) under nitrogen from 20°C (room temperature) to 220°C at the rate of 10°C/min.

High temperature gel permeation chromatography (HT-GPC)

HT-GPC analyses were performed to study the molecular weight of the PP materials. A GPC-IR6 from Polymer Char (CN1952C010) with a GMHH-R precolumn and three PLgel Olexis 3 columns was used to perform the analyses at 150°C. The columns were calibrated with polystyrene standards, and 1,2-dichlorobenzene was used as the eluent and solvent. The flow rate was 1 mL/min.

UV-Vis spectrophotometry

The optical properties of all the plastic were evaluated by recording their direct transmittance spectra in the UV-Vis range (UVB: 280-320 nm, UVA: 320-400 nm, and Vis: 400-800 nm) with a Vary Carian 500 spectrophotometer. PS, PVC, PP, PE, PC, PMMA, PET, and PPI were found to be very clear plastics in comparison with the translucent PP2. For this reason, in the case of PP2, the diffuse transmittance spectrum was also recorded.

2.2. Disinfection experiments

2.2.1. Radiation sources

Solar simulator

This system is based on a xenon lamp (Osram XBO 5000W/H XL) with a temperature colour of 6000 K located on a cinema projector with a customised reflector to ensure the adequate homogeneous illumination of the reactor (Philippe *et al.,* 2016). This system is placed at Universidad Rey Juan Carlos facilities at Móstoles, Madrid, Spain. Irradiance at the surface of the illuminated photoreaction system was measured by spectroradiometry using a calibrated StellarNet Spectrometer UVIS-25.

Atlas XLS+

An Atlas Suntest XLS+ (USA) equipped with a xenon arc lamp and a combination of filters was used as solar simulator to replicate the outdoors solar radiation spectrum. This system was placed at Universidad de Santiago de Compostela (USC, Spain). The spectral irradiance at the surface of the reaction vessel was measured with an AvaSpec-ULS2048 (200–800 nm) and with a calibrated StellarNet Spectrometer UVIS-25. This system was used to get the experimental data of *Cryptosporidium parvum* inactivation.

Atlas CPS+

Two Atlas Suntest CPS+ (ATLAS Material Testing Technology GmbH, Lisengericht, Germany) equipped with a xenon arc lamp and a combination of filters (Suprax, ATLAS, Material Testing Technology GmbH) were used to simulate the outdoor solar radiation spectrum. One was placed at the Plataforma Solar de Almería (PSA, Spain). Its spectral irradiance was measured at the surface of the reaction vessel with a radiometer PMA2100 fitted with a PMA2107 digital non-weighted UV-A+B Sensor (280-400 nm). The second

Atlas CPS+ was placed at École Polytechnique Fédérale de Lausanne (EPFL, Switzerland). The selected solar radiation intensities were set and calibrated frequently by a radiometer/pyranometer couple (CUV3/CM6b, Kipp and Zonen, Delft, Holland) and validated with a PCE-34 UV radiometer (PCE Ibérica, Spain). These systems were used to get the experimental data of MS2 and *E. coli* inactivation.

2.2.2. Reaction systems

Quartz spectrophotometric cell

A 3 mL cell was used as an optically differential photoreactor to ensure low optical density conditions, neglect radiation profiles, and assume homogeneous radiation intensity throughout its volume. This reaction system was used to evaluate the effect of ageing of plastic SODIS containers on the disinfection efficacy. For that, the aged plastic samples were located between the illumination source (solar simulator) and the frontal face of the cell. As quartz is totally transparent to UV-Vis radiation, the spectral irradiance inside the cell is exclusively affected by the plastic transmission.

Transparent Jerrycan (TJC)

25 L PET containers 525.9 mm tall and with a base of 240.5 by 262.6 mm with an average wall thickness of 0.55 mm. In Sub-Saharan Africa, plastic jerrycans of 25 L are containers universally employed for water collection and transport. Standard jerrycans are typically made of opaque PE plastic. The use of transparent jerrycans that allow the application of the SODIS process is a promising alternative and easily embraced in this region. This reaction system was used to study the effect of naturally occurring substances in water on the radiation distribution SODIS efficacy in large-volume containers. The solar simulator illuminated the TJCs under controlled conditions of UV radiance.

Vessels

Glass vessels with a total volume of 400 and 700 mL. The exterior of the vessels was completely black to avoid uncontrolled light reflections and guarantee that only the measured direct radiation incident from the top participates in the process. The clear water and the low optic path for both reaction volumes allowed considering the irradiance at the front surface as the average incident radiation in the water volume. Recirculating water baths were used to maintain a constant temperature within the vessels according to the desired experimental conditions These reaction systems were used

to obtain experimental data that allowed the modelling of the virus (vessel of 700 mL), protozoa (vessel of 400 mL), and bacteria (vessel of 700 mL) inactivation by the SODIS process.

2.2.3. Microorganisms and water composition

Escherichia coli bacteria

▶ A wild *E. coli* sp. strain was isolated from the wastewater treatment plant of Rey Juan Carlos University (Móstoles, Spain). Fresh liquid cultures were prepared by inoculation in Luria-Bertani (LB) nutrient medium and incubation at 37°C with rotary shaking for 24 h. To prepare the reaction media, 5 mL of the liquid culture were centrifuged at 3000 rpm for 15 min. Bacteria were separated from the supernatant, rinsed again with 5 mL of sterile saline solution (NaCl 0.9%), and diluted into the experimental container to obtain the initial concentration. Samples taken during the experiments were analysed using the standard serial dilution method and plating in LB agar with the colonies counted after incubation for 24 h at 37°C. The detection limit of this method was 1 CFU • mL^{-1}.

This strain was used for the experiments carried out in the differential quartz cell illuminated with the Solar Simulator. It was inoculated in deionised water with an initial concentration of 10^6 CFU • mL^4. Two sets of experiments were carried out. Firstly, experiments with the original un-aged plastic samples were used to optimise the kinetic model parameters. The second set of experiments was performed with the aged samples (8 experiments per type of plastic) to validate the kinetic model fit. The experiments were performed at a UV irradiance value of 33.0 ± 2.4 W • m^{-2} at least twice to ensure replicability. The experimental temperature was always below 30°C to avoid thermal effects on the bacteria inactivation.

Also, this strain was used for the experiments carried out in TJCs with an initial concentration of 10^3 CFU • mL^{-1} ensuring applicability to the reported typical field concentrations of 1 CFU • mL^{-1}(Abatneh ***et al.,*** 2014; Haylamicheal and Moges, 2012) or 100 CFU • mL^{-1}(Ali ***et al.,*** 2011). Experiments were carried out with tap water upon addition of sodium thiosulfate to remove residual chlorine before bacterial inoculation. Naturally occurring substances were independently added to assess the effect of the water composition on the SODIS process: iron was added as $FeSO_4$, solids and the associated subsequent turbidity was modelled using red soil whose characteristics and procedure for preparation has been described in previous studies (Castro-Alférez ***et al.,*** 2018; Ubomba-Jaswa ***et al.,*** 2010b) and sucrose was added as soluble carbohydrate to achieve the desired level of dissolved organic carbon (DOC). All parameters were independently checked at different concentration

levels with maximum initial values of 20 mg • L^{-1} of soluble carbohydrates, 100 ppm bicarbonate, 3 ppm of Fe, 20 ppm of humic acids, and 100 NTU of turbidity. All of them exceed the values commonly reported in Sub-Saharan water sources to ensure the evaluation of real conditions (Abatneh ***et al.,*** 2014; Haylamicheal and Moges, 2012). The experimental temperature was set at 25°C.

▶ A *E. coli* K12 strain was acquired from DSMZ, Germany. (Deutsche Sammlung von Mikroorganismen und Zellkulturen, Catalog No. 498) in lyophilised powder form, reactivated by the supplier's protocol. Its propagation, growth and quantification followed the procedure described for wild the wild ***E. coli.***

This strain was used to obtain experimental data of the disinfection water by the SODIS process that allowed the development of the kinetic modelling of the process. These experiments were performed in vessels of 700 mL illuminated with the Atlas CPS+ placed at the EPFL. Depending on the experiment, bacteria were inoculated in MiliQ water with an initial concentration of 10^4, 10^5, and 10^6 CFU • mL^{-1}; H_2O_2 was added into the system to a final concentration as 0, 5, 10, 30, and 50 ppm and the water temperature and UV irradiance were set as 20, 30, 40, 45, and 50°C, and 10.6, 15.0 and 20.8 W • m^{-2}, respectively. The H_2O_2 concentration in the solution was determined by the titanium oxysulfate method (DIN 38409-15).

Briefly, 20 µL of titanium oxysulfate was added in 1 mL of solution, forming a yellow complex of pertitanic acid. The absorbance of the mixture was measured using a UV-1800 spectrophotometer (Shimadzu, Japan) at 410 nm. For the experiments with bacterial debris as a sink for ROS, 15 min of boiling was performed to the corresponding ***E. coli*** concentration prior to spiking the water.

MS2 virus

MS2 coliphage (ATCC 15597B1) and the bacterial ***E. coli*** C300 171 (ATCC 15597) were used as viral model pathogen and host, respectively. Stocks of MS2 infective particles and enumeration were prepared using tryptone yeast glucose (TYG) medium containing the following reagents from Sigma-Aldrich: tryptone (10.0 g • L^{-1}), yeast extract (1.0 g • L^{-1}), NaCl (8.0 g • L^{-1}), glucose (10.0 g • L^{-1}), $CaCl_2$ (2.94 g • L^{-1}), and thiamine (0.01 g • L^{-1}); additionally, 5 and 15 g • L^{-1} of bacteriological agar was added to prepare semi-solid and solid agar medium, respectively. The ***E. coli*** host was cultivated for 6 h in fresh liquid medium at 37°C with a rotatory agitation of 90 rpm previously to MS2 enumeration. The enumeration of infective MS2 was carried out by a double-layer agar method. Briefly, 1 mL of ***E. coli*** C300 was mixed with 0.1-0.5 mL of sample (or 10-fold dilutions using Phosphate Buffer Saline) and 5 mL of melted semi-solid TYG agar. The mix was then poured on solid TYG agar

Petri dishes. Solidified plates were incubated upside-down at 37°–C for 24 h. The detection limit of this method was 2 PFU mL^{-1}.

This virus was used to obtain experimental data of the MS2 disinfection. Three sets of experiments were conducted in 700 mL vessels illuminated with the Atlas CPS+ placed at the PSA. Firstly, experiments were carried out at different water temperatures (30, 40, 45, and 50°C) under dark conditions; secondly, under different UV (280 to 400 nm) irradiances (15, 20, 30, 40, and 50 W • m^{-2}) and water temperatures (30, 40, 45, and 50°C); and, finally, the validation experiments were performed at different water temperatures and irradiances (15 and 50 W • m^{-2} of UV radiation and water temperatures of 30, 40, and 50°C) placing plastic sheets (PMMA, PP, and PET) between the photoreaction system (700 mL vessel) and the radiation source (Atlas CPS+) to change the radiation spectral distribution. Aliquots of virus stock solution were added directly into the vessel (used as photoreaction system) with autoclaved distilled water with sodium chloride (0.9% w/v) to provide an initial concentration of 10^5-10^6 Plaque Forming Units (PFU) • mL^{-1}.

Cryptosporidium parvum protozoa

Cryptosporidium oocysts were collected from a naturally infected neonatal Friesian-Holstein calf. Concentration (in 0.04 M phosphate-buffered saline [PBS] pH 7.2 and diethyl ether), purification (by discontinuous caesium chloride gradients), quantification (with a Neubauer haemacytometer) and molecular characterisation were performed as previously reported (Gómez-Couso ***et al.,*** 2012a). Briefly, faeces were collected from a calf by rectal sampling and stored at 5°C. Faecal material was then homogenised in 10-20 mL of PBS (0.04 M, pH 7.2), filtered through two sieves (mesh sizes 150 and 45 µm), shaken with diethyl ether (2:1, v/v) and concentrated by centrifugation at 2000xg, for 15 min, at 4°C. The resulting uppermost two layers were removed carefully and discarded, and the sediment was washed with PBS (0.04 M, pH 7.2) by centrifugation at 2000×g for 15 min at 4°C. *Cryptosporidium* oocysts were purified on discontinuous caesium chloride gradients of 1.05, 1.10 and 1.40 g • mL^{-1} by centrifugation at 2000×g for 30 min at 4°C. Finally, the oocysts were counted in a modified Neubauer haemocytometer, with 0.16% malachite green solution as counterstain (Kilani and Sekla, 1987; Lorenzo-Lorenzo ***et al.,*** 1993). The isolate was identified as ***C. parvum*** by PCR amplification and sequence analysis of a ≈587-bp fragment of the small subunit rDNA gene (SSUrDNA) (Ryan ***et al.,*** 2003). The viability of ***C. parvum*** oocysts was determined by inclusion/exclusion of the fluorogenic vital dye propidium iodide (PI) and a further modification that includes an immunofluorescence antibody test to verify oocyst identification (Campbell ***et al.,*** 1992; Dowd and Pillai, 1997). Briefly, 200 µL of the sediments were incubated with 15 µL of PI (Sigma-Aldrich, Co., St. Louis, Missouri, USA) working solution [1 mg • mL^{-1} in PBS (0.1 M, pH 7.2)] and 15 µL of monoclonal antibodies labelled with fluorescein iso-

thiocyanate (FITC) (AquaGlo™ G/C Direct Test, Waterborne Inc., New Orleans, Louisiana, USA), at 37°C, for 30 min (Gómez-Couso ***et al.,*** 2012a). Then, the samples were washed three times in PBS (0.04 M, pH 7.2) at 10,000×g, for 5 min at room temperature. Oocysts were identified first under a FITC filter (excitation at 450–480 nm; barrier at 515 nm) before being examined for PI inclusion/exclusion under a PI filter (excitation at 510–550 nm; barrier at 590 nm). The proportions of ruptured (ghost), PI-positive (dead), and PI-negative (viable) oocysts were quantified in an epifluorescence microscope equipped with a Nomarski differential interference contrast, FITC and PI filters (Olympus AX70, Olympus Optical Co., Ltd., Tokyo, Japan). The results are shown as the concentration of PI-negative (viable) oocysts determined for each assay after triplicate counts of more than 100 oocysts.

This protozoon was used to obtain experimental data of the ***C. parvum*** disinfection. Three sets of experiments were conducted in 400 mL vessels illuminated with the Atlas XLS+ placed at the USC. Firstly, experiments were carried out at different water temperatures (30, 40, 42, 43, 44, and 45°C) under dark conditions; secondly, under different UV (280 to 400 nm) irradiances (30, 40, and 50 W • m^{-2}) and water temperatures (30, 40, 44°C); and, finally, the validation experiments were performed at different water temperatures and irradiances (30 and 50 W • m^{-2} of UV radiation and water temperatures of 30 and 44°C) placing plastic sheets (PMMA, PP, and PET) between the photoreaction system (400 mL vessel) and the radiation source (Atlas XLS+) to change the radiation spectral distribution. The vessel with 400 mL of distilled water was spiked with 75,000 oocysts • mL^{-1} of ***C. parvum.***

2.3. Radiation transport calculations

2.3.1. Incident radiation

The photon flux density of sunlight at the solar noon ($p0_{sn}(\lambda)$) was calculated according to the following algorithm.

Firstly, the zenith angle at the solar noon should be determined. The maximum elevation angle (azimuth angle) (α) at solar noon is a function of latitude (φ) and the declination angle (δ) (Kalogirou, 2013):

$$\alpha = 90 + \varphi - \delta \qquad \text{Eq. 2.1}$$

$$\delta = 23.45^{\circ} \cdot \sin\left(\frac{360}{365} \cdot (d + 284)\right) \qquad \text{Eq. 2.2}$$

where ***d*** is the day of the year (***d*** = 1: 1 January; ***d*** = 365: 31 December).

Therefore, the zenith angle at solar noon (θ_{sn}) is given by:

$$\left(\theta_{sn}\right) = \varphi - 23.45^{\circ} \cdot \sin\left(\frac{360}{365} \cdot (d + 284)\right) \qquad \text{Eq. 2.3}$$

Once the zenith angle is defined, the relative atmospheric depth crossed by solar rays (Air mass, ***AM*$_{sn}$*)*** is calculated using the equation by Kasten and Young (1989) (**Eq. 2.4**)**.** AM is the depth of the atmospheric mantle crossed by the sun rays relative to its size when the Sun is at zenith (solar noon). Values of AM can vary from 0.0 (atmospheric depth crossed = 0) to 43.0 (maximum atmospheric depth crossed that is achieved at sunrise and sunset). Therefore, the atmospheric depth crossed at solar noon is 1.0. Note that **Eq. 2.4** is only applied for zenith angles between -90° and 90° (the zenith angles at sunrise and sunset, respectively).

$$AM_{sn} = \left(\cos\left(\theta_{sn}\right) + 0.50572 \cdot \left(90 + 6.07995 + \theta_{sn}\right)^{-1.6364}\right)^{-1} \qquad \text{Eq. 2.4}$$

Later, the irradiance that reaches Earth's surface at the solar noon ($I_{sn}(\lambda)$) is estimated applying the Lambert-Beer equation (Beer, 1852; Lambert, 1760) in which $I_{AM0}(\lambda)$ is the solar spectrum in the external layer of the atmosphere (AM=0) (Eq. 2.6):

$$I_{sn}(\lambda) = I_{AM0}(\lambda) \cdot \exp\left(-\kappa(\lambda) \cdot AM_{Sn}\right) \qquad \text{Eq. 2.5}$$

The solar spectra referred to AM 0.0 ($I_{AM0}(\lambda)$) and the atmospheric extinction coefficients (κ(∧)) can be obtained from the literature (Moreno-SanSegundo ***et al.,*** 2021). I_{sn}*(*A*)* can be easily converted to the incident spectral flux density (*p*^{0}*λ)* dividing it by , $_{h}$ being Planck's constant, ***c*** the speed of light in vacuum and ***N***$_{a}$ the Avogadro's number.

Finally, **Eq. 2.6** allows calculation of p0$_{sn}$ ***(λ)***:

$$p^{o}_{sn}(\lambda) = I_{AM0}(\lambda) \cdot \exp\left(\frac{-\kappa(\lambda)}{\cos(\phi - \delta) + 0.50572 \cdot (96.07995 + \phi - \delta)^{-1.6364}}\right) \cdot \frac{\lambda}{hc} \cdot \frac{1}{N_a} \qquad \text{Eq. 2.6}$$

where the solar spectrum that reaches the Earth's atmosphere before crossing it ($I_{AM0}(\lambda)$, AM = 0) and the atmospheric extinction coefficients κ(λ) were obtained from the literature (Moreno-SanSegundo ***et al.,*** 2021), and δ is the

sun declination angle that can be calculated as follows: (Kalogirou, 2013). Note that *dy* = 1 for 1 January and 365 for 31 December.

The day length (τ_{DL}) can be calculated with **Eq. 2.7,** which is only applicable for latitudes between 60°S and 60°N (Kalogirou, 2013):

$$\tau_{DL} = \frac{2}{15} \cdot acos(-\tan(\varphi) \cdot \tan(\delta)) \qquad \text{Eq. 2.7}$$

2.3.2. *Solar UV Calculator* tool

Microsoft Excel® software was used to develop the *Solar UV Calculator* tool to predict the total radiation available and its spectral distribution within the SODIS containers as a function of the thickness and type of plastic. For this purpose, maximum solar radiation inside the device was calculated by applying **Eq. 2.8** in the solar UV–Visible range from 290 nm to 800 nm:

$$I_{inside}(\lambda) = I_{sun}(\lambda) \cdot T(\lambda) \qquad \text{Eq. 2.8}$$

where $I_{inside}(\lambda)$ is the monochromatic radiation intensity (W • m^{-2} • nm^{-1}) inside the device, $I_{sun}(\lambda)$ the monochromatic solar radiation intensity (W • m^{-2} • nm^{-1}) and $T(\lambda)$ is the transmittance of the plastic material at each wavelength (dimensionless). The transmittance (*T*) is directly related to the absorbance (*A*) of the material (dimensionless) by the well-known **Eq. 2.9:**

$$A(\lambda) = -\log\left(T(\lambda)\right) \qquad \text{Eq. 2.9}$$

whereas the absorbance is related to optical path length (*L*) in (m) by the Beer-Lambert law **(Eq. 2.10):**

$$A(\lambda) = \beta\left(\lambda\right) \cdot L \qquad \text{Eq. 2.10}$$

where $\beta(\lambda)$ is the monochromatic extinction coefficient (m^{-1}) for wavelength λ, which depends on the material.

Based on **Eq. 2.8, Eq. 2.9** and **Eq. 2.10** the radiation intensity inside the device can be expressed as:

$$I_{inside}(\lambda) = I_{sun}(\lambda) \cdot 10\left(-Th \cdot \beta(\lambda)\right) \qquad \text{Eq. 2.11}$$

where the optical path length for the light transmission is the wall thickness of the device (*Th)* in (m).

2.3.3. Numerical simulations

Radiation transport calculations in the TJC were carried out by numerical simulations using ANSYS® Fluent v.14.5 (ANSYS Inc.) software. First, the water container was geometrically defined using the ANSYS® Workbench tool which includes three parts: i) the air outside the container, ii) the container walls with the average PET absorption coefficient in the UV range (42.14 m^{-1}) and iii) the water domain that fills the interior of the container. A boundary condition was set in one of the lateral faces of the air domain to transmit the radiation received from the light source. All the domains were meshed with a total of 228,897 volumetric cells using ANSYS® meshing tool. The number of cells was confirmed to be sufficiently high to provide mesh independent simulation results of the global incident radiation and net radiation fluxes with a relative error below of 10^{-6}.

The numerical solution of the RTE was carried out using the DOM. 15 × 15 divisions were used for the directional discretisation. All the inter-domains surfaces were set as semi-transparent and zero-thickness. As the emission of radiation can be neglected at the low operation temperatures of the process, the temperature was fixed to 1 K in all domains to inactivate calculations of radiation emission. The water (bacterial suspension and water components) was considered a pseudohomogenous medium with a refractive index of 1.33 (refractive index of water). CAT and SOD enzymes and NADH were considered as the absorption components of the bacteria. The specific absorption coefficients (κ') were obtained from the literature, using an average value in the UVA range (300-400 nm): κ^*_{CAT} as 2.6 • 10^5 M^{-1} • cm^{-1} (Castro-Alférez ***et al.,*** 2017b); κ^*_{SOD} as 800 $M^{-1}cm^{-1}$ (Jackson ***et al.,*** 2004); and κ^*_{NADH} as 6220 M^{-1} • cm^{-1} (Nakamaru-Ogiso ***et al.,*** 2010). Values of the absorption volumetric coefficients were estimated by assuming:

i) A bacterial volume of 1.96 • 10^{-13} cm^3 for a typical size of ***E.*** coli of 1 μm in length and 0.5 μm in diameter.

ii) Initial bacterial concentration of 10^3 CFU • mL^{-1}.

iii) A constant NADH concentration at the basal ***E. coli*** concentration of 2.5 • 10^{-4}M (Kishko ***et al.,*** 2012).

iv) Initial concentrations of CAT and SOD in the cell of 9.2 • 10^{-5} M (Seaver and Imlay, 2001a, 2001b) and 2 • 10^{-5}M (Imlay, 2008).

The resulting values were 3.05 • 10^{-10} cm^{-1}, \ 4.68 • 10^{-9} cm^{-1} and 3. 19 • 10^{-12} cm^{-1} for NADH, CAT and SOD, respectively. These values are sufficiently low that we can safely disregard any effect of the bacteria on the radiation field. However, absorption and scattering coefficients of water components (calculated in this work were included in the model resolution as extinction coefficients of the water. The Henyey-Greenstein phase function (Casado ***et al.,*** 2017) was included in the model as a user-defined function (UDF), using an averaged value of g_λ for the whole UVA range. All these values can be considered constant with the time as well as the radiation intensities, being solved the radiation field in steady state. The main output parameters calculated from the simulations were the average incident radiation, its uniformity index, and the average radiation flux at the rear internal face of the container.

A second-order upwind discretisation scheme was used to solve the DOM equations. The simulations were carried out using the doubleprecision solver and with standard values of the under-relaxation factors due to good convergence and reasonable computational time. Scaled residuals of the numerical solution were monitored, considering that the equations converged when residuals (relative errors) achieved a value of 10^{-6} for incident radiation and energy.

2.4. Kinetic modelling

2.4.1. Kinetic models

Three mechanistic kinetic models were developed for each type of microbial pathogen (viruses, protozoa, and bacteria). Elemental reaction steps were used to define the fundamental inactivation mechanisms.

First and second-order kinetic model

The lineal dependence of the microorganism's logarithmic concentration vs time indicates that the system is governed by a first-order kinetic model. In this case, the reaction rate is a function of the kinetic constant (*k*) and the microorganism's concentration **(*C*).** Considering that in SODIS processes in clear water the incident irradiation is constant, if the radiation participates in the reaction, the kinetic constant can be expressed as the product of another kinetic constant (k_{RAD}) and the radiation intensity (*I*) **(Eq. 2.12):**

$$\frac{dC}{dt} = k \cdot C \quad // \quad \frac{dC}{dt} = k_{RAD} \cdot I \cdot C \qquad \text{Eq. 2.12}$$

If the reaction rate depends on the concentration of two different species present in the water matrix (**A** and **B***),* the process can be defined using a second-order kinetic model **(Eq. 2.13):**

$$\frac{dC}{dt} = k \cdot A \cdot B \qquad \text{Eq. 2.13}$$

Series-event model

The presence of a shoulder in the experimental disinfection curves points to the necessity of applying a series-event kinetic model (Severin ***et al.,*** 1982). This model assumes that an event is a unit of damage, and ***n*** units of damage must be accumulated to inactivate the microorganisms. Therefore, the inactivation process takes place through a sequence of inactivation levels (***n***) guided by a first-order kinetic constant (k_1) with regard to the microorganism's concentration for each Level (C_i). Furthermore, microorganisms frequently have mechanisms that could repair damage, inducing a step backwards in the level sequence. The repair kinetic constant (k_{R-1}) can be defined as a first-order kinetic constant of the sum of the recovery mechanisms with regards to the microorganism concentration at level ***i*** (C_i). Therefore, the inactivation process takes place through a sequence of inactivation levels (***n).*** To calculate the number of microorganisms at level ***i*** ($1 \leq i \leq n$), it is necessary to account for the damaged organisms from the previous level (C_{i-1}) and the recovered organisms from the next level ***(***C_{i+1}) as a source of organisms (positive term), and the damaged and recovered organisms of the current level (C_i) as a sink of organisms (negative term). This balance is represented by **Eq. 2.14:**

$$\frac{dC_i}{dt} = k_1 \cdot C_{i-1} + k_{R-1} \cdot C_{i+1} - k_1 \cdot C_i - k_{R-1} \cdot C_i \qquad \text{Eq. 2.14}$$

Multiple target – multiple hit **model**

This model was used to account for two different sources of cumulative damage, i.e., the integration of two series-event models. If both mechanisms are considered as independent additive effects (incorporating the two series-event reactions independently), each microorganism could be taken into account as inactivated twice. Therefore, the model remembers the number of attacks of each type, avoiding the inactivation of the same microorganism by both routes.

This model was developed by Casado ***et al.*** (2021), and it is built with a 2-D matrix, one per stress source. The attack from each source moves the

microorganism one step forward in its dimension, while each independent recovery path moves the microorganism one step back. **Fig. 2.1** schematically depicts the *multiple target – multiple hit* model.

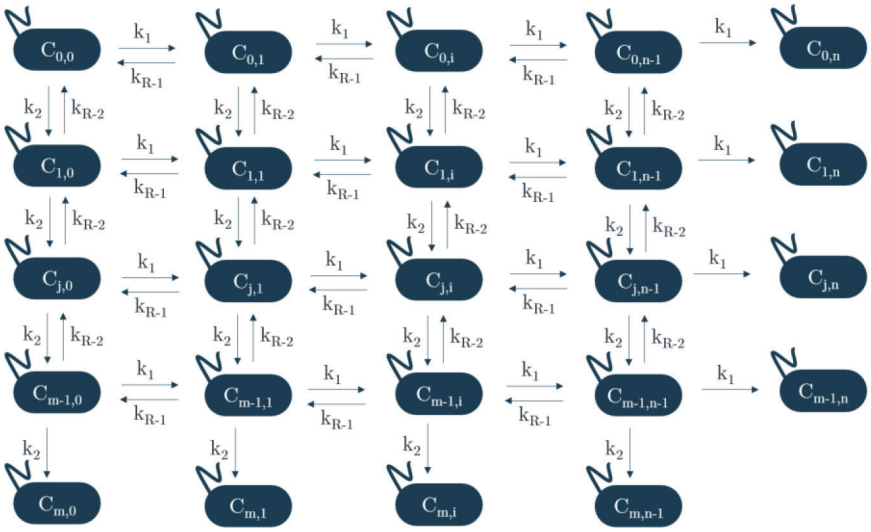

Fig. 2.1: Schematic representation of the *multiple target – multiple hit* kinetic model.

Arrhenius-like equations

The thermal effect of reaction rates, as well as the thermal inactivation of microorganisms, were modelled with Arrhenius-like equations: the typical Arrhenius equation **(Eq. 1.7)** the modified Arrhenius equation **(Eq. 1.8)** and the integration of a temperature threshold on both equations **(Eq. 1.9)**. These equations are explained in depth in **Section 1.3.3. Modelling thermal inactivation.**

2.4.2. Estimation of kinetic parameters

Once the kinetic models are mechanistically defined, the kinetic parameters of each essential reaction were obtained. For this purpose, first and foremost, the kinetic parameters already available in the literature were fixed. For missing parameters, when possible, experimental data or data from the literature were used to estimate them independently. For the remaining parameters (there is no available data or procedures to estimate them independently), a regression was performed using the normalised root mean square (logarithmic) error (NRMS(L)E) between predictions and experimental data as the objective error function. The sequential quadratic programming (SQP) optimisation method

from GNU Octave was used to minimise the error function. The system of differential equations was solved using explicit Euler. The steps followed to solve each kinetic model depended on the complexity of the global kinetic model.

Viruses

The kinetic analysis of the MS2 virus (model pathogen) inactivation was carried out through the estimation of the kinetic parameters according to the following sequential steps:

i) Dark thermal inactivation: In this case, no kinetic description was required as the experiments under dark conditions at different water temperatures resulted in negligible inactivation.

ii) UV irradiance and wavelength-dependent spectral action: Experimental data of virus disinfection under different illumination conditions at 20°C were fitted to a first-order kinetic model. The wavelength-dependent spectral action was included according to **Eq. 1.4,** and the quantum yield was calculated for this MS2 virus strain following the procedure developed by Mattle ***et al.*** (2015).

iii) Synergistic effect: Experimental data of virus disinfection under illumination conditions at different water temperatures were fitted using a modified Arrhenius equation with a threshold temperature.

Protozoa

The kinetic analysis of *Cryptosporidium parvum* inactivation was carried out through the estimation of the kinetic parameters for the different sub-models according to the following sequential steps:

i) Dark thermal inactivation: Experimental data of protozoa inactivation under dark conditions at different temperatures were fitted to a first-order kinetic model, and the effect of the water temperature on the thermal inactivation kinetic constant was modelled by the Arrhenius equation with a threshold temperature.

ii) UV irradiance inactivation: Due to the presence of a shoulder in the experiments carried out under illuminated conditions at 30°C, a series-event kinetic model was used.

iii) UV-T synergistic effect: The kinetic constant of the photonic effect was redefined with the Arrhenius equation. Experiments performed at different

conditions of UV radiation and temperature were used to obtain the kinetic parameters of the UV-T synergistic effect. Values of the kinetic parameters obtained previously were used as seeds.

iv) Wavelength-dependent spectral action: according to **Eq. 1.4** the quantum yield φ_{CP} was defined as the ratio between the number of damaged oocysts and the number of absorbed photons. To determine the rate of photon absorption, the absorption spectrum for a single oocyst was defined like Mattle ***et al.*** (2015) previously did for adenovirus, MS2, and phiX174 viruses. As Busse ***et al.*** (2019) demonstrated, absorption of solar light by ***C. parvum*** is dominated by the nucleic acid components, since the action spectrum is similar in shape to the DNA absorption spectrum, with a maximum around 260 nm. The absorbance at 260 nm can be calculated by multiplying the weight of dsDNA in ***C. parvum*** by the weight-normalised extinction coefficient of the dsDNA at 260 nm, ε_{CP}***(***260***nm),*** reported as 0.020 mL • μg^{-1} • cm^{-1} (Gallagher, 2011). The weight of the DNA of ***C. parvum*** was calculated following data deposited in National Center for Biotechnology Information (NCBI, Reference CM000429.1) (National Center for Biotechnology Information, 2020) and corresponded to 9.51×10^{-10} µg. The absorption spectrum for ***C. parvum*** was determined by considering the shape of the absorption spectrum of a ***C. parvum*** oocyst suspension measured by Busse ***et al.*** (2019).

Bacteria

The kinetic analysis of the ***E. coli*** bacteria inactivation, including the enhancement with H_2O_2 was carried out through the definition of the most representative reactions and the estimation of their kinetic parameters (**Table 3.6** and **Table 3.7**) firstly, under dark conditions, and secondly, under illuminated conditions.

1- **Dark conditions:**

The physiological and ROS-related mechanisms taking place under dark conditions were modelled using data from the literature and experimental data at different H_2O_2 concentrations and water temperatures. The steps followed were:

i) Bacteria: cell's respiration pathways and thermal inactivation

▶ R.1: O_2•- generation during cell respiration: Kinetic parameters obtained from the literature (Imlay and Fridovich, 1991)

- R.2: O_2•- scavenging by SOD: Kinetic parameters obtained from the literature (Zheng ***et al.,*** 2007)

- R.3: H_2O_2 scavenging by CAT: Kinetic parameters obtained from the literature (Castro-Alférez ***et al.,*** 2017b)

- R.4 and R.5: Internal Fenton and Fenton-like processes: R4: kinetic data from the literature fitted to a second-order kinetic model and an Arrhenius equation (Park ***et al.,*** 2005), R5: kinetic parameters estimated by model regression (MD-1).

- R.6, R.7, and R.8: radicals' recombination: Kinetic parameters obtained from the literature (Buxton ***et al.,*** 1988), (Gallard and De Laat, 2000), and (Buxton and Elliot, 1993), respectively.

- R.9 and R.10: bacterial damage by O_2•- and HO• radicals: seriesevent model used according to the literature (Casado ***et al.,*** 2021) and kinetic constants recalculated by model regression (MD-1).

- R.11: Dark thermal inactivation: experimental data ***(E. coli*** disinfection profiles at different water temperatures without H_2O_2) fitted to a first-order kinetic model and an Arrhenius equation.

ii) H_2O_2: thermal decomposition

- R.A: H_2O_2 decomposition: experimental data (H_2O_2 profiles at different water temperatures without bacteria) fitted to a first-order kinetic model and an Arrhenius equation.

iii) Interaction between H_2O_2 and bacteria

- R.B: H_2O_2 permeation: kinetic data obtained from the literature (Seaver and Imlay, 2001b)

- R.C: Membrane-H_2O_2 interaction: Data from the literature (H_2O_2 profiles at different temperatures with porinless ***E. coli,*** (Feng ***et al.,*** 2020)) fitted to a second-order kinetic model.

- R.D: Organic Matter from killed cells-H_2O_2 interaction: experimental data (H_2O_2 profiles at different water temperatures with 10^6 CFU • mL^{-1} of bacteria boiled to produce the cellular lysis) fitted to a first-order kinetic model and an Arrhenius equation.

2- **Illuminated conditions**

The mechanism under light conditions was modelled using data from the literature and experimental data at different H_2O_2 and ***E. coli*** initial concentrations, water temperatures, and UV solar light conditions. The steps followed were:

i) Cellular photoinactivation

- R.12: O_2• generation under light: kinetic parameters estimated by model regression (MD-2).
- R.13: SOD deactivation: kinetic parameters estimated by model regression (MD-2).
- R.14: CAT deactivation: kinetic data from the literature fitted to a first-order kinetic model (Castro-Alférez ***et al.,*** 2017b)
- R.15: Internal Photo-Fenton: kinetic data obtained from the literature (Casado ***et al.,*** 2021)
- R.16-1: Direct DNA damage (at 20°C): This effect was modelled with a series-event model but was coupled to the series-event model of the radicals' attacks using the ***multiple target – multiple hit*** model according to the literature (Casado ***et al.,*** 2021) and the kinetic constants were recalculated by model regression (MD-2).

ii) UV-T synergistic effect:

- R.16-2: Direct damage + UV-T synergy: kinetic constant from R.16-1 was redefined with the Arrhenius equation. Kinetic parameters were obtained by model regression (MR-3).

In order to reduce the number of variables to estimate at the same time, three regression steps were defined:

- MR-1: This model regression just considered the reactions that occur under dark conditions (from R.1 to R.11 and from R.A to R.D). All the experiments carried out under dark conditions were used to run this first model regression.
- MR-2: This model regression took into account the reactions that occur under dark conditions and under illuminated conditions at 20°C (from R.1 to

R.11 and from R.A to R.D, and from R.12 to R. 16.1). All the experiments performed under illuminated conditions at 20°C were used to run this second model regression.

- MR-3: This model regression accounted for all the reactions of the mechanistic model and studied conditions (R.16-1 was changed by R.16-2). All the experiments performed under illuminated conditions at any water temperature were used to run this third model regression.